The Influence of Surface Charges on the Conductance of the Human Connexin37 Gap Junction Channel

K. Banach, S. V. Ramanan, and P. R. Brink
Department of Physiology and Biophysics, State University of New York at Stony Brook, Stony Brook, New York 11794 USA

ABSTRACT The single-channel conductance of the hCx37 homotypic gap junction channel does not saturate with transjunctional voltages up to ±75 mV, nor does it depend linearly on the intracellular electrolyte concentration. The average maximum unitary conductances measured in KCl were 175 pS (30 mM), 236 pS (55 mM), 343 pS (110 mM), and 588 pS (270 mM) in the presence of 0.1 mM $MgCl_2$. The unexpectedly high unitary conductance at low salt concentrations can be explained by fixed charge groups within or near the channel orifice. Fixed cytoplasmic surface charges (3.4 *e*) positioned adjacent (15 Å) to the channel pore adequately model the data (surface charge density of 0.24 $e/(nm)^2$). In other experiments, high Mg^{2+} reduced the unitary conductance of hCx37 homotypic gap junction channels more than predicted by screening alone, consistent with specific effects of Mg^{2+} on the channel.

INTRODUCTION

Gap junction channels are a pathway for ions and second messengers between the cytoplasmic compartments of adjacent cells (Tsien and Weingart, 1976; Harris et al., 1981; Brink, 1996). The channel is composed of two hemichannels, one provided by each of the connected cells. Six protein subunits, connexins, assemble to form a hemichannel. More than 13 different proteins that belong to this connexin gene family have been identified (Goodenough et al., 1996; Nicholson et al., 1993). The connexin family exhibits a high overall homology and four transmembrane domains are predicted based on hydropathic studies. However, the homotypic channels formed by the different connexins vary in their single-channel conductance by a factor of 10 (Veenstra et al., 1995).

In general, the conductance of a channel depends on its entrance or access region, its diameter, length, and possible binding sites or selectivity filter(s) inside or near the region of the pore. Previous studies have shown that gap junctions can pass up to 1200-Da dye molecules and discriminate only weakly between anions and cations (Simpson et al., 1977; Veenstra et al., 1994, 1995; Wang and Veenstra, 1997; Brink, 1996). The hypothesis that fixed charges influence the permeability of gap junctions was proposed for gap junctions in the earthworm septate median giant axon (Brink and Dewey, 1980; Verselis and Brink, 1986). For anionic dyes it was shown that permeation rate declined with increased charge density. Furthermore, the zwitterionic dye molecule aminofluorescein, despite its small size, exhibited a low permeation rate and reduced the permeability of other monovalent dyes. Similar proposals have been made for mammalian gap junction channels (Veenstra et al., 1994). The aim of our investigation was to determine whether fixed charges near or within the pore of homotypic Cx37 channels were effective in influencing unitary channel conductance.

Received for publication 21 July 1999 and in final form 10 November 1999.
Address reprint requests to Dr. Peter R. Brink, Dept. of Physiology/Biophysics, SUNY Health Science Center, Stony Brook, NY 11794. Tel.: 516-444-3124; Fax: 516-444-3432; E-mail: peter@patch.pnb.sunysb.edu.
© 2000 by the Biophysical Society
0006-3495/00/02/752/09 $2.00

METHODS

All of the experiments were performed on neuroblastoma cells (N2a) transfected with cDNA for hCx37 (Reed et al., 1993), using the double whole-cell patch clamp technique (DWCP, Neyton and Trautman, 1985). The standard pipette solution used as a reference contained (in mM): 110 KCl, 1 EGTA, 0.1 $CaCl_2$, 1.8 $MgCl_2$, and 10 HEPES (pH 7.1). The corresponding standard bathing solution contained (in mM): 110 KCl, 1 $CaCl_2$, 1.8 $MgCl_2$, and 10 HEPES (pH 7.1–7.3). In order to obtain a conductance concentration curve, the concentration of the main salt (KCl) in the bathing and the pipette solution was changed from 110 mM to 270, 180, 150, 55, or 30 mM. We found that N2a cells are able to volume-regulate in bathing solutions with an osmolarity up to 3.75 times that of the standard solution (230 mOsm). For those solutions where the KCl concentration was below the standard, namely the 30 mM and the 55 mM KCl solutions, sucrose was added to bring the final osmolarity up to the standard of 230 mOsm. When testing for the effects of Mg^{2+} on the conductance, $MgCl_2$ was added to the 110 KCl solution at concentrations of 0.1 and 1.8 mM, or to the 55 mM KCl pipette solution at concentrations of 0.1 and 5 mM. In all these experiments the dishes containing plated N2a cells were perfused with bathing solution and allowed to sit for at least 15 min before patching.

The experiments can broadly be divided into two categories: macroscopic experiments, where the number of junctional channels is $>\sim 10$, and few-channel experiments, where up to three junctional channels are present. For the macroscopic experiments, the voltage protocol was applied by a computer either with the Labmaster hardware (Scientific Instruments, Inc., New York, NY) and the pClamp software suite (Axon Instruments, Inc., Foster City, CA) or with a DT21EZ board (Data Translation, Inc., Boston, MA) and custom software. The resultant macroscopic currents from both cells were stored directly on the computer at a sampling rate of 1 ms after filtering at 500 Hz with a 4-pole Bessel filter (LPF-30, World Precision Instruments, Inc., Hamden, CT). For few-channel experiments, the steps were applied manually through the front panel of the Axon patch clamp amplifiers, filtered at 1 KHz, digitized at 14 bits (Neurocorder, Mentor, OH), and stored on videotape.

Macroscopic records were obtained with the method given in Brink et al. (1997). In brief, the voltage pulses were applied to one cell, here called $cell_1$ of a cell pair; the junctional current was obtained by monitoring the nonstepped cell ($cell_2$), which was held at $V_m = 0$ mV. One protocol

commonly used was as follows: after a step from 0 mV to 10 mV for 100 ms and a return to 0 mV for 100 ms, 400-ms pulses of voltages from −150 to 150 mV in 20-mV steps were applied to $cell_1$; $cell_2$ was held throughout at 0 mV. After these 400-ms voltage pulses, the voltage polarity in $cell_1$ was reversed and finally returned to 0 mV. A second protocol was identical to the one above, except that the time scale was greater by a factor of 10, i.e., pulses were 4 s long rather than 400 ms. The current was recorded in both cells. For simplification only the current in the recipient cell ($cell_2$), which reflects the transjunctional current (I_j) is shown in the figures of the Results section. In the text, we refer to this protocol as the standard protocol.

In weakly coupled cell pairs single-channel data could be recorded. All records were obtained by stepping $cell_1$ to various holding potentials while holding $cell_2$ at 0 mV. Before this, the offset potential on the patch clamp amplifiers were adjusted so that both amplifiers passed zero current at an apparent holding potential of 0 mV. The records that were analyzed were all taken from $cell_2$ of a cell pair. The current that is injected into $cell_2$ is reduced from the true junctional current by approximately the ratio of pipette to cell resistance, when the seal resistance is high. All experiments here had this ratio greater than 50 to 1 for both cells; then the measured junctional current from $cell_2$ is within 2% of the true value from $cell_1$. As a check on these predictions, we have measured the magnitude of some of the transitions in single-channel currents from the stepped cell for every record presented here. In some records the magnitude of the current transition in $cell_2$ was as much as 40% smaller than that in $cell_1$. We do not have an explanation for this phenomenon. We have simply removed all records where the difference in current steps from $cell_1$ and $cell_2$ was >10% from consideration. After correcting for the measured drop in current from $cell_1$ to $cell_2$, the conductance remained very stable across records (SD 5%) and it is this corrected conductance that we present in the Results. Note that there is a difference between applied and true holding potentials for the same reason; however, we have not corrected for this. The conductances presented here therefore are lower bounds on the true conductance.

To avoid the problems associated with series resistance in high conductance pairs (Wilders and Jongsma, 1992) we have not studied data sets where the apparent junctional conductance was >10–20 times the pipette series resistance. This puts an upper limit of ~75 hCx37 channels in all the macroscopic records shown here. hCx37 shows transitions from its maximal conducting (or main open) state to a subconductance state and rarely shuts to 0 pA, the true closed state. This is reflected both in the transition currents and peak-to-peak distance measured in amplitude histograms. The subconductance state is the lesser conductance state (see Veenstra et al., 1994). There are many subconductance states possible, but for hCx37 the most frequently observed (or dominant) subconductance state has a conductance of 50–100 pS depending on the salt concentration (Veenstra et al., 1994). Henceforth, the usage of the term substate without any qualification refers to this dominant substate. Throughout the text, reference to unitary conductance will be made using the following terms: maximal unitary conductance, main transition step, and subconductance. Thus, maximal unitary conductance (γ) = main transition step + subconductance (e.g., 343 pS = 285 pS + 58 pS in 110 mM KCl). The main transition step is the difference between the substate conductance and the maximal unitary conductance.

In a number of experiments low salt concentrations were used that resulted in elevated pipette resistances. Large pipette resistances that are comparable to the intercellular resistances result in poor voltage clamping, which will result in an apparent increase in V_0 (Wilders and Jongsma, 1992). However, both pipette resistance and intercellular resistance increase proportionally with the resistance of the salt solution, and their ratio stays constant over different salt concentrations. If increased series resistance resulted in poor voltage clamping, the measured conductance in the low salt concentrations would be disproportionately lower than measured conductance in normal or higher salt concentrations. The conductance-concentration curve would round off for low concentrations, but in fact the data in low salt exhibit the opposite phenomenon (see the Results section).

RESULTS

Macroscopic hCx37 gap junction channel currents

The current through hCx37 gap junction channels depends on the transjunctional voltage (V_j). Junctional current traces obtained in $cell_2$ of a cell pair during the application of the standard voltage protocol (see Methods) are shown in Fig. 1 *A*. Transjunctional voltages >30 mV induce a decline of the current over the duration of the pulse; this V_j-dependent reduction of the hCx37 junctional current results in a non-zero steady-state level which is reduced relative to the instantaneous junctional currents. Half-maximal inactivation occurs between 30 and 40 mV (see Fig. 1 *B*.) Instantaneous junctional current increases linearly with V_j ($\pm$100 mV). The instantaneous junctional conductance is then deemed to be constant and indicates that the instantaneous unitary conductance of hCx37 is not rectifying as V_j increases.

Human Cx37 single-channel current increases in proportion to V_j

In a number of experiments ($n = 5$) where only one or a few hCx37 channel(s) were observed, a 4-s step of 25 mV was applied and near the end of the step a voltage ramp (0.54 mV/ms) was applied to a peak of $V_j = 90$ mV over 120 ms, followed by a ramp (−0.54 mV/ms) back to 25 mV. The last second of such a trace is shown in Fig. 2. The top trace shows the V_j profile and the junctional current reveals a main transition. The application of the ramp occurred while the channel was in the dominant substate. There is a subsequent transition to the open state, and the junctional current followed the voltage ramp to $\sim V_j = 75$ mV before the transition to the substate. Note that the current of the main open state follows V_j linearly. Using this protocol it was not possible to observe the main open state at voltages higher than 70–90 mV due to the voltage-dependent gating of hCx37 to the substate. However, the linear increase of junctional current during the voltage ramp correlates well with the linear dependence of the instantaneous current on V_j observed in macroscopic records. Although the figure is also consistent with linearity of the substate current with V_j (the shallower dark line is the prediction for linearity), the short duration of the substate data and the potential presence of other additional substates makes it impossible to be dogmatic about this point. Nevertheless, these data clearly indicate that there is no voltage-dependent saturation of the maximal unitary conductance of the hCx37 gap junction channel, at least up to a V_j of 75 mV.

Concentration conductance relationship of hCx37

In a number of experiments we varied the intracellular concentration of permeable ions to obtain a concentration-

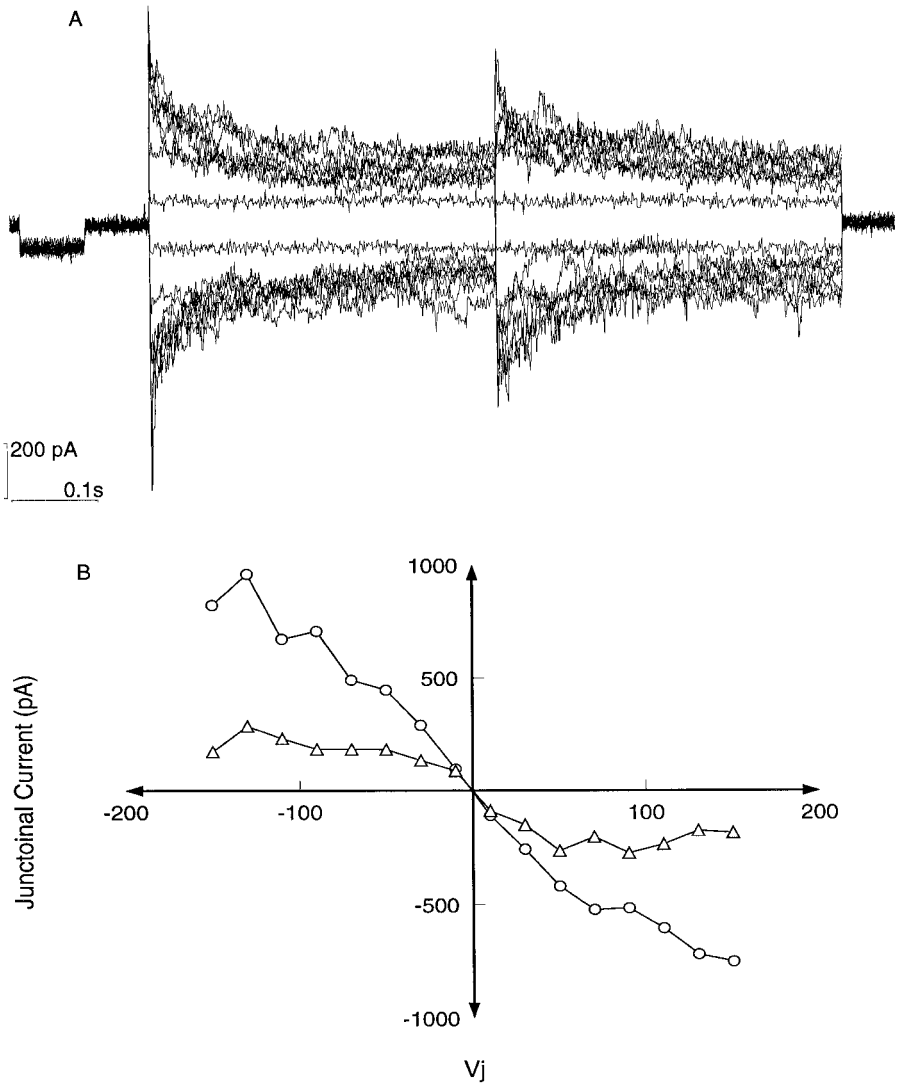

FIGURE 1 (A) Current traces recorded in the nonpulsed cell during the application of a standard protocol to one cell of a cell pair. (*B*) Instantaneous and steady-state *I-V* curves are plotted. The instantaneous junctional current increases linearly with applied voltage; the steady-state *I-V* curve reflects the effects of voltage-dependent decline in junction current.

conductance plot. The single-channel conductance of hCx37 was determined in 30, 55, 110, 150, 180, and 270 mM KCl. At least five experiments were performed for each salt concentration. Representative current traces recorded in 30, 110, and 270 mM KCl are shown in Fig. 3. The top tracing shows unitary channel activity of hCx37 channels in 30 mM KCl, where V_j was -40 mV. The main transition was 142 pS. In the middle panel the main transition was 260 pS in 110 mM KCl; here V_j was -25 mV. The bottom panel illustrates the case where V_j was -20 mV and the KCl concentration was 270 mM. For this case the main transition was 480 pS. For all three cases shown there are at least two active channels. In the bottom panel the dominant subconductance associated with hCx37 is illustrated. I_j is 0 pA at the beginning of the record, but in the latter portion of the trace the dominant subconducting state can be seen (Veenstra et al., 1994).

The data from all the experiments are summarized in Fig. 4. In this figure the single-channel conductance associated with the main transition step is plotted as a function of the intracellular salt concentration. The inset shows a plot of the dominant substate conductance against KCl concentrations for 110, 180, and 270 mM KCl. The substate data were taken from one or a few channel recordings where direct transitions to $I_j = 0$ were observed. The number of such recordings are $n = 1$ for 270 mM, $n = 3$ for 180 mM, and $n = 1$ for 110 mM. A linear fit of the dominant substate conductance against concentration was linear with a slope conductance of 0.31 pS/mM ($r = 0.9x$). For [KCl] = 55 or 30 mM, we were unable to obtain records that showed direct transitions to $I_j = 0$. Hence we have taken the data from the other concentrations and extrapolated to 55 and 30 mM.

For the main transition conductance the relationship shows a weak tendency to saturate at high concentrations. This phenomenon, which is well described for voltage-dependent membrane channels, can be explained by the rate theory of permeation (Hille, 1992). Somewhat more notable is the observation that in salt concentrations of 30 mM and

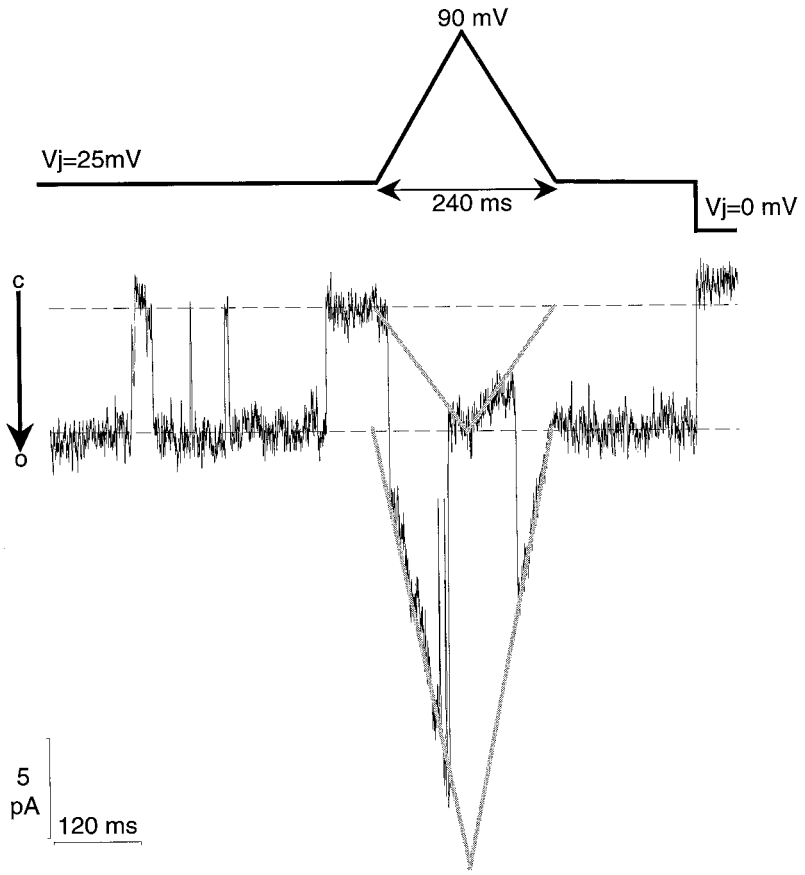

FIGURE 2 Single-channel recording (*bottom*) in a weakly coupled cell pair (V_j = +25 mV). A voltage ramp is applied after 4 s, increasing the transjunctional voltage to +90 mV. Single-channel conductance follows the ascending voltage with 2.7 pA/ms. The top panel shows the transjunctional voltage profile used. Both main transition conductance and dominant subconductive states can be seen in this record.

55 mM KCl, the single-channel conductance remains high. This is an indication that charges in the entranceway of the channel pore might influence the local concentration of counterions (Green and Anderson, 1991). In effect, the increased cloud of ions provides a ready pool of permeating ions whose local concentration is higher than the bulk solution concentration. A method of modeling the effect of a spherically symmetric distribution of surface charges near the mouth of a pore has been described in Naranjo et al. (1994). This method has the advantage over the Gouy-Chapman formalism in that it allows determination of both the number and the distance of these surface charges from the pore mouth. The minor tendency to saturation at high concentrations has been modeled phenomenologically by a Michaelis-Menten relation. This combination of the Michaelis-Menten formalism and the linearized model of surface charge is illustrated in Eq. 1 below:

$$\frac{\gamma}{\gamma_{max}C} = \frac{e^{-A\exp(-B\sqrt{C})}}{C\,e^{-A\exp(-B\sqrt{C})} + K_d} + \frac{e^{A\exp(-B\sqrt{C})}}{C\,e^{A\exp(-B\sqrt{C})} + K_d} \quad (1)$$

In Eq. 1, A is defined as 1.43 q/a and B by 3.28 a, where q is the surface charge (in units of e, the electronic charge), which is modeled as a uniformly distributed hemispherical layer as described above (Naranjo et al., 1994). This hemisphere is at a distance of a nm from the channel mouth. K_d is the Michaelis-Menten half-saturation constant, γ_{max} is the conductance for large concentrations of salt, and C is the concentration of the major salt. The data were fitted for the total maximal conductance γ of the channel (main transition step + dominant subconductance) assuming that the subconductance depends linearly on the salt concentration as indicated in Fig. 4. The solid line in Fig. 4 represents the best fit with this model (Levenberg-Marquardt optimization) with the following values for the parameters: a = 1.52 nm, q = 3.42 e, γ_{max} = 768 pS, and K_d = 433 mM. The effective charge density σ in a Gouy-Chapman formalism is $\sigma = q/(2\pi a^2) = 0.24\ e/(\text{nm})^2$.

We have noted above that no substate data could be collected at 30 and 55 mM. The total maximal conductance at these lower salt concentrations may then not be an accurate value. If the true substate conductance were greater than predicted from linear extrapolation this would further increase the maximal channel conductance at low concentration, and the surface charge density required by the model to fit the data would only increase. Consider the opposite case, where the substate conductance at low concentrations is assumed to be zero. Constraining the distance from charge to channel mouth to be 1.52 nm, the best fit parameters are q = 2.22 e, γ_{max} = 709 pS, and K_d = 377 mM. The effective charge density σ = 0.16 $e/(\text{nm})^2$ decreases as

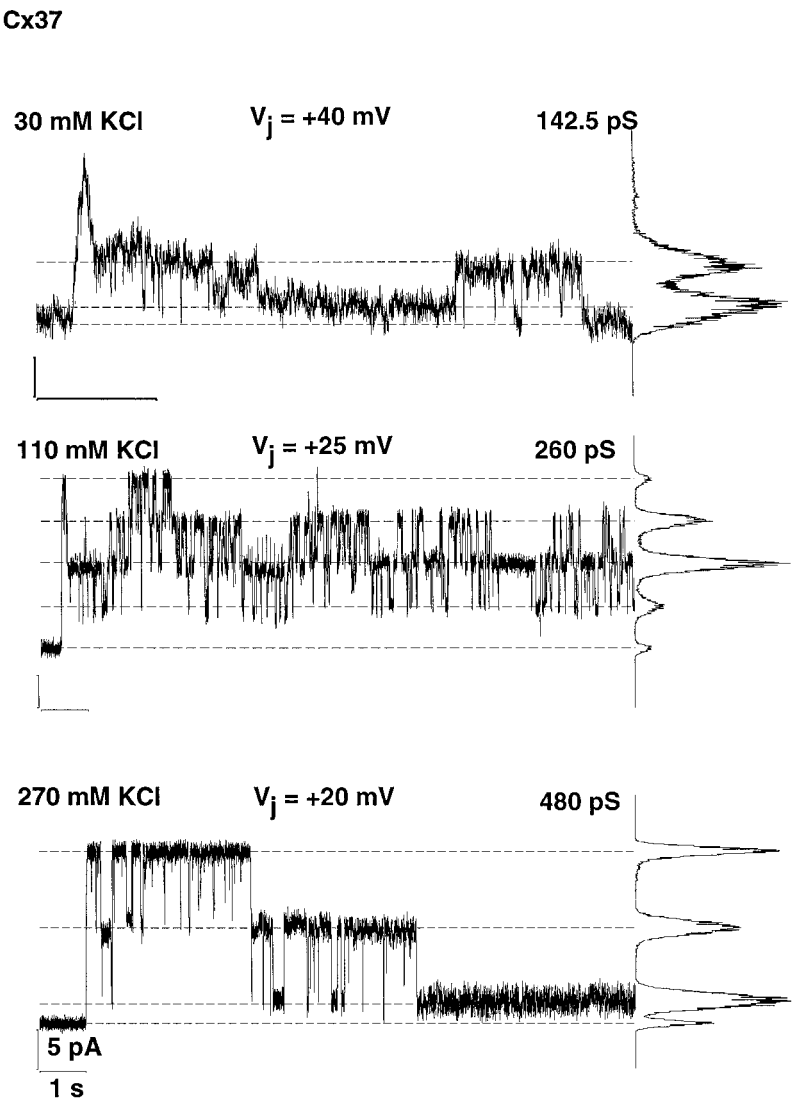

FIGURE 3 Single-channel events recorded in cell pairs with different salt concentrations (30, 110, and 270 mM) KCl. *Top panel:* 30 mM, $V_j = -40$ mV; *middle panel:* 110 mM, $V_j = -25$ mV; *bottom panel:* 270 mM, $V_j = -20$ mV.

expected. For comparison, the average charge density of a membrane with 20% charged lipids in 100 mM NaCl is 0.12 $e/(\text{nm})^2$ (Ohki and Kurland, 1981).

Mg^{2+} influences the single-channel conductance of hCx37

The influence of surface charges depends on the intracellular salt concentration, especially on the concentration of divalent ions (McLaughlin, 1977). To probe this we changed the intracellular concentration of $MgCl_2$. Experiments were carried out with 110 mM KCl and 0.1 or 1.8 mM $MgCl_2$, respectively. The conductance recorded for the main transition was 280 and 295 pS, respectively. However, elevating the intracellular concentration from 0.1 to 5 mM $MgCl_2$ in the 55 mM KCl pipette solution resulted in a drop of the main transition step from 195 to 110 pS.

Use of the Gouy-Chapman formalism and the Grahame equation (MacKinnon et al., 1989 and Appendix) enabled us to calculate the theoretical influence of increasing concentrations of divalent ions on the conductance. This method had to be used in place of the formalism underlying Eq. 1, as that method is not easily extended to divalents. The underlying assumptions are that the surface charges are uniformly smeared over the membrane and that the effect of divalents is solely due to the nonspecific screening of those charges. The equation was solved assuming the charges were located at a distance of either 0 or 15 Å from the pore entrance; there was little difference between the fits for the optimized parameters. The calculated data are presented in Fig. 5 (for 0 Å) and represent the total conductance of the channel. Experimentally derived values for maximal conductance and dominant subconductance under varied Mg^{2+} conditions and KCl concentration are also shown.

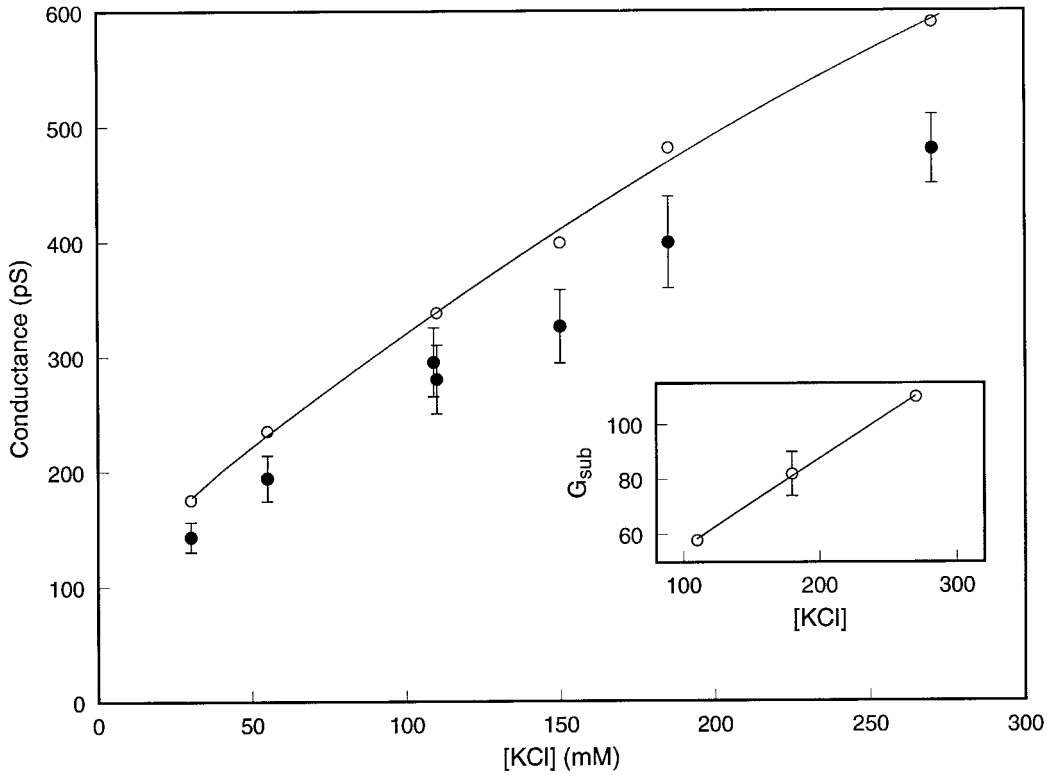

FIGURE 4 Concentration versus conductance plot for hCx37. Main transition step (●) and dominant subconductance state (*inset:* slope conductance of 0.31 pS per mM) were treated independently. The data represent the mean ± SD. The maximal single-channel conductance (○) (main transition step + subconductance) was obtained assuming that the subconductance depends linearly on the salt concentration. The solid lines represent a fit of the data to a model combining aspects of saturation and surface charges.

Assuming that the intracellular solution contains 110 mM KCl and ≤0.1 mM $MgCl_2$, the maximal conductance (main transition step + subconductance) calculated would be 339 pS. Recall that the main transition step is ~285 pS and the subconductance is 58 pS, resulting in a maximal conductance of 343 pS. An increase of the intracellular $MgCl_2$ concentration to 10 mM does not appreciably change the predicted maximal conductance (339 pS for 0.1 mM, 338 pS for 1.8 mM, and 337 pS for 10 mM). The surface charges seem to be sufficiently titrated by the concentration of monovalents such that even an increase to 1.8 or 10 mM $MgCl_2$ does not significantly reduce the predicted maximal conductance. The experimental data are in agreement with theory for 0.1 mM and 1.8 mM Mg^{2+} where the maximal conductances were 343 and 353 pS, respectively.

The deviation between theory and experiment occurs when Mg^{2+} is elevated to 10 mM. The predicted maximal conductance is 337 pS and the experimentally determined value is 203 pS (175 pS, main transition, $n = 4$; 28 pS, substate, $n = 1$). The experimental data exhibit a greater drop in conductance than predicted by screening alone in the 10 mM case. A binding site for Mg^{2+} is one possible explanation.

Comparison of predicted values and experimental data with 55 mM KCl leads to similar conclusions. In these low intracellular salt concentrations, a drop in the single channel maximal conductance from 230 pS to 214 pS is predicted by the calculations when 5 mM $MgCl_2$ is added to the solution. The experimental values of the main transition step were 195 pS in 0.1 mM $MgCl_2$ and 110 pS in 5 mM $MgCl_2$. We did not attempt to determine the conductance of the subconductance state directly, but the linear relationship shown in Fig. 4 extrapolates to 41 pS at 55 mM KCl. Thus the maximal conductance is 235 pS in 0.1 mM $MgCl_2$ and 151 pS in 5 mM $MgCl_2$, with the KCl concentration at 55 mM. Here again the experimental data reveal a greater drop in conductance than predicted, indicating that screening by Mg^{2+} is not the only mechanism of its action, and that other specific effects of Mg^{2+} are involved. Unfortunately, determining the nature of the exact mechanism of Mg^{2+} effects on the conductance is beyond the scope of this study.

DISCUSSION

The shape of the concentration conductance curve obtained for hCx37 is consistent with the hypothesis that the channel conductance is modulated by surface charges located in the vicinity of the pore entrance. The channel conductance also

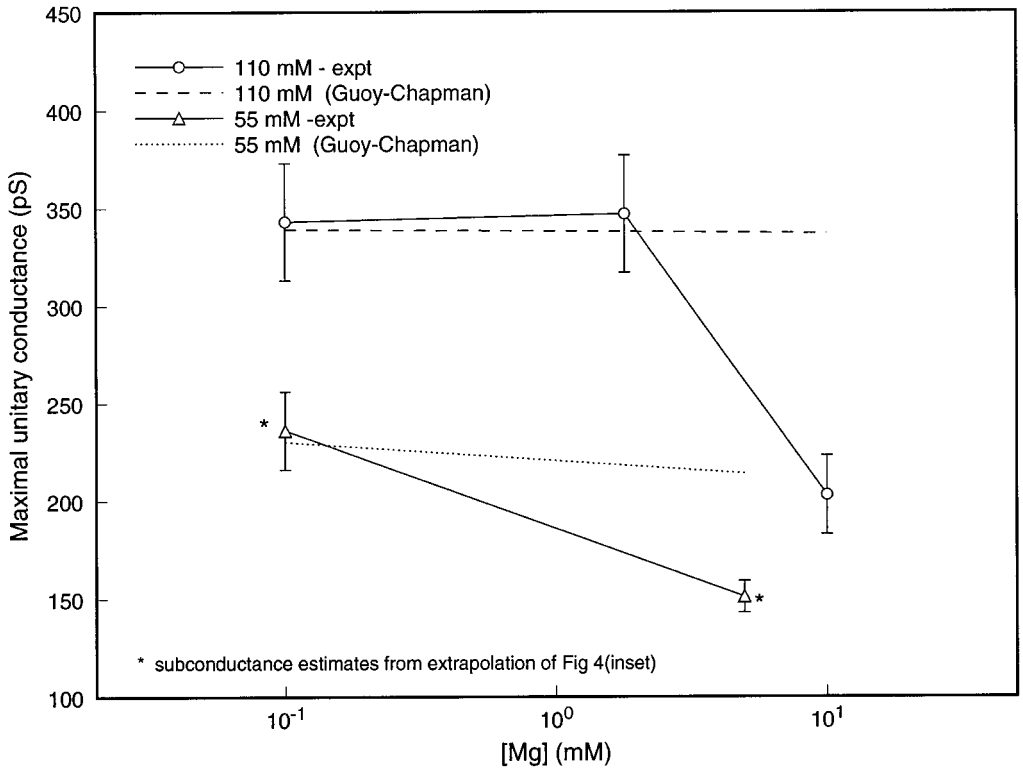

FIGURE 5 Conductance of hCx37 channels plotted against pipette [Mg] with 55 and 110 mM KCl solution in the pipette. The dotted lines are predictions from a Gouy-Chapman screened charge model whose parameters are derived from fits of the conductance-[KCl] data in Fig. 4. The observed reduction in conductance with [Mg] is greater than predicted from nonspecific screening effects of magnesium alone, suggesting that magnesium has specific effects on the channel conductance.

shows a weak tendency to saturate with increased intracellular salt concentrations, although not with transjunctional voltage.

The primary observation is that the conductance of the single hCx37 channel stays high with low KCl concentration. Examination of the conductance-concentration curve in Fig. 4 shows that the curve when linearly extrapolated shows a non-zero conductance in the zero-concentration limit. Similar observations in other channels (Green and Anderson, 1991) have been interpreted as evidence for charges in the pore mouth, i.e., as a surface charge effect.

Charges located on the membrane or on channel proteins induce electrostatic potentials and alter the surrounding ionic environment. These fields increase with decreasing salt concentrations, since the surface charge becomes more effective in attracting counterions in low salt concentrations. Thereby it increases the local counterion concentration over that of the bulk solution. The influence of charges in these conditions is signaled by the observation of high single-channel conductances at low salt concentrations. We fitted the concentration conductance curve with a combination of the Michaelis-Menten equation and the linearized form of a surface charge model (Naranjo et al., 1994). The model tries to account for the effectiveness of charges near the entrance of the pore by modeling the charge distribution as hemispherical around the mouth of the channel. The best fit of the concentration-conductance curve of hCx37 was obtained with 3.42 charges localized in a hemisphere with a radius of 15 Å, with a surface charge density $\sigma = 0.24$ $e/(\text{nm})^2$. With these parameters, the model predicts that the local concentration of monovalent cations increases by a factor of 2.3 in 110 mM KCl and 3.1 in 55 mM KCl. These results indicate that surface charges are a viable explanation for the unusually high conductances of hCx37 channels observed in low salt solutions.

Adding divalents to the pipette solutions should efficiently titrate the surface charge and provide a test of the surface charge hypothesis. However, adding $MgCl_2$ to the pipette at concentrations of 10 mM (in 110 mM KCl) or 5 mM (in 55 mM KCl) decreased the channel conductance far more than would be expected from the charge screening mechanism alone. The data thus appear to require another mechanism of Mg^{2+} action, such as specific binding, partial channel blockade, or a change of selectivity. Other specific effects of Mg^{2+} on hCx37 channel gating have been observed (Ramanan et al., 1999).

A question that we have not addressed is whether ion-ion interaction inside the channel can account for this anomalous behavior. Evidence for ion-ion and ion-channel interaction has been shown in other gap junction channels (Hu and Dahl,

1999; Musa and Veenstra, 1999). Conventionally, ion-ion and ion-channel interactions become manifest at high salt concentrations (Hille, 1992), while the phenomenon observed here is prominent at low salt concentrations, e.g., 30 mM. Assuming 1) a channel with diameter 1.2 nm (Veenstra et al., 1995) and a length of 100 nm; 2) no surface charge effects; and 3) that the concentration in the channel pore is the same as that in the pipette solution, the number of ions in the channel lumen is 0.75 for a salt concentration of 30 mM. If the hCx37 data are to be interpreted as evidence for ion-ion interaction in the channel, however, the average number of ions in the channel should be ~2. Such an increase in the average ion number from 0.75 (at 30 mM) to 2 is then also consistent with a surface charge that increases the ion concentration near the channel mouth. We are thus led to the conclusion that while we cannot discount ion-ion interaction inside the channel, we are still obliged to assume surface charge at or near the channel mouth to explain the data at low concentrations.

Would unitary conductance of a nonselective channel be affected by surface charge? Gap junction channels have been shown to be poorly selective, allowing the passage of both cations and anions (Veenstra et al., 1994; Brink, 1996). It would seem, at first sight, that a (negative) surface charge would increase the cation concentration and decrease the anion concentration near the channel mouth, and hence for a poorly selective channel the total conductance would not be greatly altered. For simplicity, assume the channel is completely nonselective, i.e., equally permeable to anions and cations. Further assume that the increase in exposed negative surface charge due to a reduction in the salt concentration results in a doubling of the cation concentration near the pore mouth and a halving of the anion concentration. This would result in the unitary conductance increasing from 2 (units) to 2.5 (units), an increase of 25%. In this example, for a highly selective cation channel, the unitary conductance would increase from 1 (unit) to 2 (units), i.e., by 100%. The difference between selective and nonselective channels, in terms of the effects of surface charge, is a difference in the magnitude of the surface charge needed to produce the same effect.

Charges that influence the conductance of a channel can be part of the lipid membrane or can originate from the channel protein itself. Although the lipid membrane of mammalian cells contains 20% of charged lipids, a direct influence on the single-channel conductance has not been demonstrated. For example, incorporation of sodium and potassium channels into neutral lipid bilayers did not abolish the dependence of their conductance on surface charges (MacKinnon et al., 1989).

In any case, for the hCx37 gap junction channel, charged lipids do not seem a plausible explanation. This is because rat Cx43 (rCx43), another gap junction protein expressed in the same N2a cell system, has a linear concentration conductance relationship (Banach et al., 1998). Assuming that the overall structure of gap junction channels remains similar, charged lipids would presumably affect the conductance through both hCx37 and rCx43 in the same way. Furthermore, the distance of the charges predicted by Eq. 1 indicates that the charges derive from the channel protein itself, since x-ray diffraction studies predict an outer diameter of 66 Å for the protein (Unger et al., 1997). Cai and Jordan (1990), in modeling the influence of variously placed charges on the single-channel conductance, proposed that the charges are most effective when they are located a the bottom of a funnel-shaped entranceway. Orientations like this are predicted for the nAChR channel and the sodium channel (Imoto et al., 1988).These analogies again suggest that the surface charges that affect conductance in hCx37 could be localized in the protein. Furthermore, work on other connexins (Cx26 and Cx32) by Verselis et al. (1994) has indicated that charged protein residues near the N-terminus have effects on the gating behavior of connexins.

The experiments described here do not allow the determination of the polarity of the surface charges. However, experiments obtained with hCx37 in heterotypic conformation with rCx43 exhibit rectification with an increasing conductance when the hCx37 side is more positive (Brink et al., 1997). The sidedness of the rectification is consistent with the assignment of negative polarity to the surface charges on the hCx37 protein, which induces a locally asymmetric ion concentration at the entrance regions of the heterotypic channel.

APPENDIX

The conductance data at various KCl concentrations from 30 mM to 270 mM with a low (0.1 mM) concentration of divalent Mg^{2+} was treated as if it were obtained in a divalent-free solution. A modification of Eq. 1 in the main text was used; here the Gouy-Chapman theory of a lumped surface charge density parameter was combined with a Michaelis-Menten equation. This was optimized to fit the conductance-concentration curve for various assumed distances L of smeared charge from pore entrance. Specifically (see, e.g., McLaughlin, 1977 or MacKinnon et al., 1989),

$$\psi(0) = 50 \sinh^{-1}(137\sigma/\sqrt{C})$$

$$\psi(L) = 50 \ln\left\{\frac{1 + \alpha \exp(-\kappa L)}{1 + \alpha \exp(-\kappa L)}\right\}$$

$$\alpha = \frac{\exp(\psi(0)/50) - 1}{\exp(\psi(0)/50) + 1} \tag{A1}$$

$$[K]_L = [K]_\infty \exp(-\psi(L)/25)$$

$$[Cl]_L = [Cl]_\infty \exp(\psi(L)/25)$$

$$\gamma/\gamma_{max} = \frac{[K]_L}{[K]_L + K_d} + \frac{[Cl]_L}{[Cl]_L + K_d} \tag{A2}$$

where $\psi(L)$ is the potential (in mV) at distance L (in Å) from the surface with charge density σ (in charges/A^2). For a given distance L of charge from pore mouth, there are three adjustable parameters, namely the Michaelis-Menten half-saturation concentration K_d (in molar), the charge density σ, and the saturating conductance γ_{max} (in pS). The fact that K_d is identical for potassium and chloride, and the fact that ions are formally

identically treated in the equation for the conductance, implies that we are considering a completely nonselective pore. The notation $[K]_L$ indicates the potassium concentration (in molar) at distance L from the smeared charge, and similarly $[Cl]_L$ for chloride. The symbol C stands for the monovalent concentration in the pipette; in the absence of divalents we have $K_\alpha = Cl_\alpha = C$. The experimental data were fitted to optimize three adjustable parameters for $L = 0$ and $L = 15$ Å. For $L = 0$, the optimized parameters are $\sigma = 1.036 \times 10^{-3}$ Å^{-2}; $\gamma_{max} = 947$ pS, and $K_d = 0.627$ M. For $L = 15$ Å, the fit to the experimental data is only sightly worse than for $L = 0$ Å; the optimized parameters are $\sigma = 4.384 \times 10^{-3}$ Å^{-2}, $\gamma_{max} = 684$ pS, and $L_d = 0.355$ M.

In the presence of divalents, the boundary conditions in the form of the Grahame equation can still be integrated. Given the charge density σ, this equation

$$\sigma^2 = \Delta(0)$$

where

$$\Delta(x) = C(e^{-\psi(x)/25} - 1) + (C + C_2) \cdot (e^{\psi(x)/25} - 1) + C_2(e^{-2\psi(x)/25} - 1)$$

is solved iteratively for $\psi(0)$. Here C_2 is the concentration of $MgCl_2$ and C is the concentration of KCl.

However, the entire Gouy-Chapman differential equation cannot be integrated. The boundary condition for $\psi(0)$ obtained above is used to numerically integrate this equation

$$\psi[x] = 0.328\sqrt{\Delta(x)}$$

for $\psi(x)$ in the region from 0 to L, and the potential $\psi(L)$ is thereby obtained. Given the potential at the pore mouth $\psi(L)$, the concentrations of ions at the mouth, and the associated conductance can be determined from Eq. (A2). These results are presented in Fig. 5.

Finally, we note that the calculations were repeated for a pore that is selective for potassium alone; however, there was no significant change in the major results embodied in Fig. 5, namely that the channel conductances in the presence of magnesium cannot be explained on the basis of nonspecific screening alone.

The authors thank Dr. E. C. Beyer for providing the cells and E. Peterson for technical assistance.

This work was supported by National Institutes of Health Grants HL31299 and GM 55263, and a BASF postdoctoral fellowship to K. Banach.

REFERENCES

Banach, K., S. V. Ramanan, and P. R. Brink. 1998. Homotypic hCx37 and rCx43 and their heterotypic form. *In* Gap Junctions. R Werner, editor. IOS Press, Amsterdam.

Brink, P. R. 1996. Gap junction channel gating and permselectivity: their roles in coordinated tissue function. *Clin. Exp. Pharm. Physiol.* 23:1041.

Brink, P. R., K. Cronin, K. Banach, E. Peterson, E. M. Westphale, K. H. Seul, S. V. Ramanan, and E. C. Beyer. 1997. Evidence for heteromeric gap junction channels formed from rat connexin43 and human connexin37. *Am. J. Physiol.* 273:C1386–C1396.

Brink, P. R., and M. M. Dewey. 1980. Evidence for fixed charge in the nexus. *Nature.* 285:101–102.

Cai, M., and P. C. Jordan. 1990. How does vestibule surface charge affect ion conduction and toxin binding in a sodium channel? *Biophys. J.* 57:883–891.

Goodenough, D. A., J. A. Goliger, and D. L. Paul, 1996. Connexins, connexons, and intercellular communication. *Annu. Rev. Biochem.* 65: 475–502.

Green, W. N., and O. S. Anderson, 1991. Surface charges and ion channel function. *Annu. Rev. Physiol.* 53:341–359.

Harris, A. L., D. C. Spray, and M. V. L. Bennett. 1981. Kinetic properties of a voltage dependent junctional conductance. *J. Gen. Physiol.* 77:95–117.

Hille, B. 1992. Ionic Channels of Excitable Membranes. 2nd Ed. Sinauer Associates, Sunderland, MA. 362–389.

Hu, X., and G. Dahl. 1999. Substitution of amino acid L35 in connexin46 results in change of channel permeability. *Biophys. J.* 76:220*a*. (Abstr.).

Imoto, K., C. Busch, B. Sakmann, M. Mishina, T. Konno, J. Nakai, H. Bujo, Y. Mori, K. Fukuda, and S. Numa. 1988. Rings of negatively charged amino acids determine the acetylcholine receptor channel conductance. *Nature.* 335:645–648.

MacKinnon, R., R. Latorre, and C. Miller, 1989. Role of surface electrostatics in the operation of a high-conductance Ca^{2+}-activated K^+ channel. *Biochemistry.* 28:8092–8099.

McLaughlin, S. 1977. Electrostatic potentials at membrane-solution interfaces. *Curr. Top. Membr. Transp*. 9:71–135.

Musa, H., and R. D. Veenstra. 1999. Ionic blockade of the rat connexin40 ionic permeation pathway by tetraalkylammonium ions. *Biophys. J.* 76:221*a*. (Abstr.).

Naranjo, D., R. Latorre, D. Cherbvaz, P. McGill, and M. F. Schumaker. 1994. A simple model for surface charge on ion channel proteins. *Biophys. J.* 66:59–70.

Neyton, J., and A. Trautmann. 1985. Single-channel currents of an intercellular junction. *Nature.* 317:331–335.

Nicholson, B. J., T. Suchyna, L. X. Su, P. Hammernick, F. L. Cao, C. Fourtner, L. Barrio, and M. V. L. Bennett. 1993. Divergent properties of different connexins expressed in Xenopus oocytes. *Progr. Cell Res.* 3:3–13.

Ohki, S., and R. Kurland. 1981. Surface potential of phosphatidylserine monolayers. II. Divalent and monovalent ion binding. *Biochim. Biophys. Acta.* 645:170–176.

Ramanan, S. V., P. R. Brink, K. Varadaraj, E. Peterson, K. Schirrmacher, and K. Banach. 1999. A three-state model for connexin37 gating kinetics. *Biophys. J.* 76:2520–2529.

Reed, K. E., E. M. Westphale, D. M. Larson, H. Z. Wang, R. D. Veenstra, and E. C. Beyer. 1993. Molecular cloning and functional expression of human Cx37. *J. Clin. Invest.* 91:997–1004.

Simpson, I., B. Rose, and W. R. Loewenstein. 1977. Size limit of molecules permeating the junctional membrane channels. *Science.* 195:294–296.

Tsien, R., and R. Weingart. 1976. Inotropic effect of cAMP in calf ventricular muscle studied by a cut-end method. *J. Physiol.* 61:829.

Unger, V. M., N. M. Kumar, N. B. Gilula, and M. Yaeger. 1997. Projection structure of a gap junction membrane channel at 7 Å resolution. *Nat. Struct. Biol.* 4:39–43.

Veenstra, R. D., H. Z. Wang, D. A. Beblo, M. G. Chilton, A. L. Harris, E. C. Beyer, and P. R. Brink. 1995. Selectivity of connexin-specific gap junctions does not correlate with channel conductance. *Circ. Res.* 77: 1156–1165.

Veenstra, R. D., H. Z. Wang, E. C. Beyer, S. V. Ramanan, and P. R. Brink. 1994. Connexin37 forms high conductance gap junction channels with subconductance state activity and selective dye and ionic permeabilities. *Biophys. J.* 66:1915–1925.

Verselis, V. K., and P. R. Brink. 1986. The gap junction channel: its aqueous nature as indicated by deuterium oxide effects. *Biophys. J.* 50:1003–1007.

Verselis, V. K., C. S. Ginter, and T. A. Bargiello. 1994. Opposite voltage gating polarities of two closely related connexins. *Nature.* 368:348–351.

Wang, H. Z., and R. D. Veenstra. 1997. Monovalent ion selectivity sequences of the rat connexin43 gap junction channel. *J. Gen. Physiol.* 109:491–507.

Wilders, R., and H. J. Jongsma, 1992. Limitations of the dual voltage clamp method in assaying conductance and kinetics of gap junction channels. *Biophys. J.* 63:942–953.